

In-Beam Diamond Start Detectors

M. Ciobanu*, E. Berdermann, N. Herrmann, K.D. Hildenbrand, M. Kiš, W. Koenig, J. Pietraszko, M. Pomorski, M. Rebisz-Pomorska, A. Schüttauf

Abstract—This paper describes operation principles and the in-beam performance of Start Detector (SD) assemblies consisting of Diamond Detectors (DDs) grown by Chemical Vapour Deposition (CVD) and Front End Electronics (FEE) which have been designed for and used in various nuclear physics experiments at GSI Helmholtz Center for Heavy Ion Research in Darmstadt.

In parallel to the FEE design we have performed extensive calculations to model the dependence of the signal-to-noise ratio (S/N) and the time resolution σ_t on various quantities such as the collected charge Q_{col} , the detector capacitance C_D , the temperature T , and finally the noise contribution and bandwidth of the amplifier.

In combination with the new FEEs (including an application-specific integrated circuit, ASIC) we have tested both polycrystalline and single-crystal diamonds of various sizes and thicknesses with relativistic ion beams ranging from protons to heaviest ions.

For heavy ions all setups deliver time resolutions $\sigma_t < 60$ ps. In case of protons the small primary detector signals require single-crystals as material and more elaborated designs like segmentation of the detector area and the increase of the amplifier input impedance. The best time resolution obtained for relativistic protons was $\sigma_t = 117$ ps.

Index Terms—Detector instrumentation, Analog integrated circuits, Timing circuits, Timing electronics

I. INTRODUCTION

An in-beam Start Detector (SD) is an important component of Time-of-Flight (TOF) systems, which are commonly used to identify different reaction products in fixed-target nuclear physics experiments. It provides the time-zero

Manuscript received September 24, 2010; revised February 10, 2011 and April 17, 2011; accepted June 05, 2011. This work was supported in part by the European Community through the FP6 Integrated Infrastructure Initiative Hadron Physics, Proj. RI3-CT-2004-506078 and in part by the German BMBF under the project number 06HD154.

M. Ciobanu is with the GSI Helmholtz Zentrum für Schwerionenforschung GmbH, 64291 Darmstadt, Germany. He is also with the Space Sciences Institute, 077125 Bucharest, Romania (email: m.ciobanu@gsi.de).

E. Berdermann, K. D. Hildenbrand, W. Koenig and A. Schüttauf are with the GSI Helmholtz Zentrum für Schwerionenforschung GmbH, 64291 Darmstadt, Germany (e-mail: e.berdermann@gsi.de; k.hildenbrand@gsi.de; w.koenig@gsi.de; a.schuettauf@gsi.de).

N. Herrmann is with the Physikalisches Institut der Universität Heidelberg, 69120 Heidelberg, Germany (e-mail: N.Herrmann@gsi.de).

M. Kiš is with the GSI Helmholtz Zentrum für Schwerionenforschung GmbH, 64291 Darmstadt, Germany. He is also with the Ruder Bošković Institute, 10000 Zagreb, Croatia (email: m.kis@gsi.de).

J. Pietraszko is with the Institut für Kernphysik der Johann Wolfgang Goethe Universität Frankfurt, 60438 Frankfurt am Main, Germany (email: j.pietraszko@gsi.de).

M. Pomorski and M. Rebisz-Pomorska are now with the Diamond Sensor Laboratory of CEA-LIST Saclay, F-91191 Gif-sur-Yvette, France (e-mails: M.Pomorski@cea.fr, M.Rebisz@cea.fr).

Color versions of one or more of the figures in this paper are available online at <http://ieeexplore.ieee.org>.

Digital Object Identifier 10.1109/TNS.2011.2160282

(T_0) or reference time for the TOF measurement by determining the crossing time of each beam particle before it hits the target. So the uncertainty in T_0 affects directly the TOF resolution and hence the velocity and the mass identification [1]. In order to reach TOF resolutions below 100 ps, the time resolution σ_t of the SD must be below the half of that value. In addition, another feature may be of importance: high beam intensities require fast detectors delivering narrow signals and electronics which can cope with the corresponding rates. In connection with this the material should be radiation hard to withstand high integral doses without sizeable degradation of its properties.

In the next section we describe briefly the physical parameters of diamonds, which make them an almost ideal active detector material to meet the mentioned requirements.

A prerequisite, however, is an optimal adaptation of the used FEE. In order to understand better the underlying relations and dependencies of parameters, such as the signal-to-noise ratio S/N and the time resolution σ_t on various system parameters, we have performed model calculations the results of which have influenced especially the design of the detectors for minimum-ionizing protons.

Formalism and the results are described in section III. We start with the simplest model of readout electronics (just one resistor) to evaluate the dependence of S/N and σ_t on the collected charge Q_{col} , on the detector capacitance C_D and on the temperature T . In a few steps we add the contribution of the amplifier noise and its bandwidth, resulting in a set of analytical formulae describing the dependence of S/N and σ_t on these parameters. Two extreme cases are discussed: The hypothetically instantaneous charge collection and the more realistic case of charge drift to the opposite electrodes. In section IV we present several SD-setups, which have been designed for different experiments, and their resolutions σ_t which have been achieved with various beams of relativistic ions.

All diamonds used in the present studies have been grown at Element Six Ltd. (King's Ride Park, Ascot, Berkshire SL58BP, UK) and supplied by DIAMOND DETECTORS LTD (16 Fleetsbridge Business Centre, Upton Road, Ponte, Dorset BH17AF, UK). We investigated both types: polycrystalline diamond detectors (pcDD) grown on silicon wafers and single-crystal diamond detectors (scDD) grown on mono-crystalline {100}-oriented High-Pressure-High-Temperature (HPHT) synthetic diamond substrates.

II. CVD DIAMONDS AS DETECTOR MATERIAL

In comparison to any other known detector material, diamond features a high mobility for both carriers, which can be derived from the field-dependent carrier drift velocities $\nu(E)_{e,h}$ measured with broadband amplifiers (BBA) applying the Transient Current Technique (TCT) with short-range α -particles [2]. Note that the FWHM of the TCT signals represents the carriers transition time $t_{tr} = d/\nu(E)_{e,h}$ with the detector thickness d , whereas the signal area corresponds to Q_{col} . The directly measured mobility values obtained by one of the authors for scDD at lowest possible electric fields E_D are $\mu_e = 1800 \text{ cm}^2/\text{Vs}$ and $\mu_h = 2450 \text{ cm}^2/\text{Vs}$ at $E_D = 0.1 \text{ V}/\mu\text{m}$ and $E_D = 0.06 \text{ V}/\mu\text{m}$, respectively [3]. These mobilities in conjunction with very high breakdown fields $E_{break} > 10^7 \text{ V/cm}$ and a low dielectric constant $\epsilon_r = 5.7$ provide detector signals of fast rise times and narrow pulse widths suitable for fast timing and counting of high ion rates. Moreover, diamond is radiation hard [4], most likely due to the high atomic packing factor of the carbon atoms in the diamond lattice causing strong covalent bonds. The same origin compels a wide band gap ($E_g = 5.48 \text{ eV}^{T=300\text{K}}$), which provides diamond sensors of very low dark current but also of high pair production energy $\epsilon_{Dia} \approx 13 \text{ eV}$, and thus of relatively low sensitivity, e.g. compared to silicon ($\epsilon_{Si} \approx 3.6 \text{ eV}$). Its thermal conductivity ($20 \text{ Wcm}^{-1}\text{K}^{-1}$), which is six times higher than that of copper, supports self-annealing of shallow traps and protects in-beam detectors against thermal spikes.

In scDDs, practically 100% of the generated primary charge is collected. In pcDD a part of this charge is lost at grain boundaries resulting in reduced charge collection efficiencies $CCE = Q_{col}/Q_{gen}$ between 0.1 and 0.6 (with Q_{gen} the ion generated charge). Due to the current production technology however, the size of standard scDDs do not exceed $5 \text{ mm} \times 5 \text{ mm}$, which is given by the dimensions of the HPHT diamond substrates used for the epitaxial growth. The maximum area available so far may reach $10 \text{ mm} \times 10 \text{ mm}$.

For precise calculations of the amplitudes of signals emitted by relativistic heavy ions in diamond sensors of different quality, the transient current signal shape has to be known; such simulations are not available at present. Hence, we estimated roughly the pulse heights delivered by two diamond detectors (DD) of $300 \mu\text{m}$ thickness on the 50Ω input impedance of a BBA, taken into account signal widths (FWHM) of 2.5 ns and 1.5 ns for a scDD ($CCE = 1$) and a pcDD ($CCE = 0.4$), respectively [5].

The results plotted in Fig. 1 have been calculated for particles of 1 A GeV kinetic energy. The horizontal solid line indicates the equivalent noise amplitude of the diamond broadband amplifier (DBA) [6], i.e. $\sigma_{nDBA} \approx 50 \mu\text{V}$, whereas the dashed line the $3\sigma_{nDBA}$ deviation noise amplitude. Fig. 1 illustrates the large dynamic range of signals expected in hadron physics experiments. Furthermore, it shows that the BBA readout in the case of relativistic ions lighter than carbon is challenging even for spectroscopic grade single-crystal diamond sensors.

III. HOW CAN THE DETECTION OF RELATIVISTIC PROTONS BE IMPROVED?

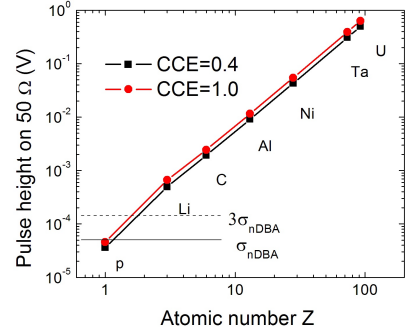


Fig. 1. Estimated pulse heights on the input of a BBA. The data have been calculated for various relativistic heavy ions of a kinetic energy of 1 A GeV traversing two DDs of $d = 300 \mu\text{m}$ and $CCE = 0.4$ and 1.0 , respectively.

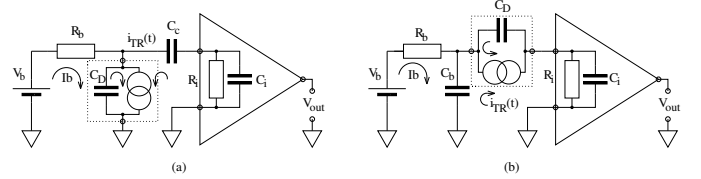


Fig. 2. Schematic layout of two circuits for the connection of a DD to its amplifier (see text for explanation).

Fig. 2 shows the two FEE schematics, which are most frequently used to read out DDs: (a) one DD electrode is connected to ground; the second one is biased and read out, (b) one electrode is biased, the second one read out. The bias is applied by the power supply V_b via resistor R_b . In mode (b), the capacitor C_b decouples the biasing resistor thus eliminating its thermal noise. Due to the high volume resistivity of the material, the breakdown voltage is very high and the leakage current at nominal operation bias is negligible. The equivalent schematic comprises a pure capacitor and a current generator.

A. Signal Processing at Instantaneous Collection of Charge

In the following we will calculate the S/N using the simplified schematics shown in Fig. 3. The diamond detector is connected to the simplest measurement system represented by the resistor R_i . This approach is similar to: "S/N versus Capacitance in a Current-Sensing Amplifier" [7], [8] and we will continue with the evaluation of the time resolution σ_t .

This schematics represents a low pass filter with a time constant $\tau_S = R_i C_D$ and a cut-off frequency $f_S = 1/(2\pi\tau_S)$.

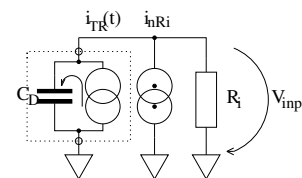


Fig. 3. Simplified equivalent schematic for noise estimations: the detector (dashed box) is connected to a simple measurement device represented by the resistor R_i .

For simplicity it is assumed that the induced current is a delta pulse $\delta(t)$ carrying the total collected charge Q_{col} ,

$$\int_{-\infty}^{\infty} i_{TR}(t)dt = \int_{-\infty}^{\infty} Q_{col} \cdot \delta(t)dt = Q_{col},$$

whereas the current discharging of the capacitor C_D is given by

$$i_C(t) = I_0 e^{-t/\tau_S}. \quad (1)$$

The charge conservation law predicts,

$$Q_{col} = \int_0^{\infty} i_C(t)dt = I_0 \cdot \tau_S$$

so that

$$i_C(t) = Q_{col}/\tau_S \cdot e^{-t/\tau_S}. \quad (2)$$

The peak current at $t = 0$, corresponds to the signal V_s

$$V_s = R_i \cdot i_C(0) = Q_{col}/C_D, \quad (3)$$

so that

$$v_{S\delta}(t) = Q_{col}/C_D \cdot e^{-t/\tau_S}. \quad (4)$$

Equation (4) is the amplitude response to the input delta pulse $\delta_I(t)$. The noise power P_n generated in a passive resistor depends on temperature (T) and bandwidth (Δf):

$$P_n(T, \Delta f) = 4 \cdot K \cdot T \cdot \Delta f = i_{nRi}^2 \cdot R_i,$$

with the Boltzmann constant K , i_{nRi} being the thermal current noise generator describing the noise generated in R_i

$$i_{nRi}^2/\Delta f = 4 \cdot K \cdot T/R_i. \quad (5)$$

For the evaluation of the noise voltage V_{Nin} we take into account the current density $i_{nRi}^2/\Delta f$ and the complex impedance $Z(f)$, which results from the parallel connection of R_i and C_D :

$$V_{Nin}^2(f) = \frac{i_{nRi}^2}{\Delta f} \cdot |Z(f)|^2 = \frac{i_{nRi}^2}{\Delta f} \frac{R_i^2}{1 + f^2/f_S^2}.$$

By the integration from $f = 0$ to ∞ we obtain the total noise of the system given in (6)

$$V_{Nin}^2 = \frac{i_{nRi}^2}{\Delta f} \cdot R_i^2 \cdot f_S \cdot \frac{\pi}{2} = K \cdot T/C_D. \quad (6)$$

From (3) and (6) we obtain the S/N ratio:

$$S/N = Q_{col}/\sqrt{K \cdot T \cdot C_D}. \quad (7)$$

In the simplified approach of Fig. 3, the S/N depends only on Q_{col} , $C_D^{-1/2}$ and $T^{-1/2}$. In the derivation the signal voltage peak V_s is assumed at $t = 0$. However, in real time measurements we have to consider the time when the signal crosses the discriminator threshold. The charge generation in a DD is much faster than the time constant of any actual amplifier. The limited rise time of the amplifier affects the time resolution (σ_t) [9]–[11]:

$$\sigma_t = \frac{\sigma_n}{dv/dt}. \quad (8)$$

where σ_n is the noise dispersion and dv/dt the signal slope (SL) at the discrimination level. The maximum slope at the amplifier output can be estimated to $dv/dt = 0.8 \cdot V_s/t_{rA}$,

where t_{rA} is the amplifier rise time (10% to 90% amplitude level). For an amplifier with a single pole and the frequency bandwidth BW_A one obtains $t_{rA} = 0.35/BW_A$ and $dv/dt = 0.8 \cdot V_s/t_{rA} = 2.28 Q_{col} \cdot BW_A/C_D$. Hence we can rewrite (8) as follows:

$$\sigma_t = \frac{\sqrt{K \cdot T/C_D}}{2.28 \cdot Q_{col} \cdot BW_A/C_D} = \frac{\sqrt{K \cdot T \cdot C_D}}{2.28 \cdot Q_{col} \cdot BW_A}. \quad (9)$$

It has been assumed that the noise dispersion is equal to the noise voltage V_{Nin} estimated in (6). Concluding, the simple schematic of Fig. 3 allows the estimation of the maximum performance that can be reached in terms of S/N or σ_t . It also outlines the importance of the reduction of the total capacitance including the diamond capacitance, the amplifier input capacitance and parasitic capacitances of the setup.

This discussion can be extended to a more accurate definition of the noise contribution of a BBA connected to a DD. In RF applications, the noise factor parameter F is used to describe the ratio of the total noise at amplifier output related to the noise contribution of the source resistor R_s :

$$F = \frac{e_{nRs}^2 + e_{neq}^2}{e_{nRs}^2}. \quad (10)$$

(Note that data sheets normally use the Noise Figure parameter NF , which is related to F by $NF = 10 \log F$ (dB)). We can estimate the noise contribution of the amplifier according to

$$e_{neq}^2 = (F - 1) \cdot e_{nRs}^2$$

or translated in noise current values, as given in 11)

$$i_{neq}^2 = (F - 1) \cdot i_{nRs}^2. \quad (11)$$

If we can consider R_i in Fig. 3 as a noiseless resistor we can modify (5) to obtain i_{neq} , i.e. the noise generator which represents the total noise contribution of the amplifier:

$$i_{neq}^2/\Delta f = 4K \cdot T \cdot (F - 1)/R_i \quad (12)$$

and the final expressions for the S/N (7) and σ_t (9) are

$$S/N = Q_{col}/\sqrt{K \cdot T \cdot (F - 1) \cdot C_D} \quad (13)$$

and

$$\sigma_t = \frac{\sqrt{K \cdot T \cdot (F - 1) \cdot C_D}}{2.28 \cdot Q_{col} \cdot BW_A}. \quad (14)$$

As expected, the use of low noise amplifiers is mandatory for both good S/N ratio and time resolution.

In (13) the "shaping" effect of the BBA is not specified, whereas in (14) only the slope limitation is estimated. In the following we will try a more accurate approach. Considering that the BBA has the low frequency gain G_0 and the gain-frequency dependence $G_A(f)$ of a single pole of cut-off frequency f_A ,

$$|G_A(f)| = \frac{G_0}{\sqrt{1 + f^2/f_A^2}}. \quad (15)$$

The noise voltage at the amplifier output is

$$\begin{aligned} V_{Nou}^2(f) &= \frac{i_{nRi}^2}{\Delta f} \cdot |Z(f)|^2 \cdot |G_A(f)|^2 \\ &= \frac{i_{nRi}^2}{\Delta f} \cdot \frac{R_i^2 \cdot G_0^2}{(1 + f^2/f_S^2) \cdot (1 + f^2/f_A^2)}. \end{aligned} \quad (16)$$

By integration of (16) from $f = 0$ to ∞ we obtain the total noise at the amplifier output (17)

$$\begin{aligned} V_{Nou}^2 &= \frac{i_n^2 R_i}{\Delta f} \cdot R_i^2 \cdot G_0^2 \cdot f_S \cdot \frac{f_A}{f_S + f_A} \cdot \frac{\pi}{2} \\ &= \frac{K \cdot T \cdot (F - 1) \cdot G_0^2}{C_D \cdot (1 + \tau_A/\tau_S)} = \frac{K \cdot T \cdot (F - 1) \cdot G_0^2}{C_D \cdot (1 + m)}, \end{aligned} \quad (17)$$

where $m = \tau_A/\tau_S$. The response $v_{A\delta}(t)$ of the amplifier to the delta function excitation $\delta(t)$ is

$$v_{A\delta}(t) = V_A \cdot e^{-t/\tau_A}, \quad (18)$$

with

$$\int_0^\infty v_{A\delta}(t) dt = V_A \cdot \tau_A = G_0. \quad (19)$$

For the evaluation of the output signal, we have to use the convolution of the signal $v_{S\delta}(t)$ developed on R_i (3) with $v_{A\delta}(t)$ given in (18):

$$\begin{aligned} v_{out}(t) &= v_{S\delta}(t) \otimes v_{A\delta}(t) = \int_{-\infty}^\infty v_{S\delta}(u) v_{A\delta}(t-u) du \\ &= V_S \cdot V_A \cdot e^{-t/\tau_A} \cdot \int_0^t e^{u(1/\tau_A - 1/\tau_S)} du. \end{aligned}$$

a) for the particular case of $\tau_A = \tau_S$

$$v_{out}(t) = V_S \cdot V_A \cdot e^{-t/\tau_A} \cdot t = \frac{Q_{col}}{C_D} \cdot \frac{G_0}{\tau_A} \cdot e^{-t/\tau_A} \cdot t. \quad (20)$$

$v_{out}(t)$ has a maximum for $t_M = \tau_A$

$$v_{out}(t_M) = \frac{Q_{col}}{C_D} \cdot \frac{G_0}{e}.$$

b) for $\tau_A \neq \tau_S$

$$v_{out}(t) = \frac{Q_{col}}{C_D} \cdot G_0 \cdot \frac{\tau_S}{\tau_S - \tau_A} \cdot (e^{-t/\tau_S} - e^{-t/\tau_A}). \quad (21)$$

$v_{out}(t)$ is maximal for

$$t_M = \frac{\ln \frac{\tau_A}{\tau_S}}{1/\tau_S - 1/\tau_A} = \tau_A \frac{\ln m}{m - 1}. \quad (22)$$

If we can measure the peak value $v_{out}(t_M)$ by peak detection we find

$$v_{out}(t_M) = \frac{Q_{col}}{C_D} \cdot G_0 \cdot \frac{1}{1 - m} \cdot \left(e^{\frac{m \cdot \ln m}{1 - m}} - e^{\frac{\ln m}{1 - m}} \right) \quad (23)$$

$$V_{Nou} = G_0 \cdot \sqrt{\frac{K \cdot T \cdot (F - 1)}{C_D \cdot (1 + m)}}. \quad (24)$$

We can calculate the S/N ratio;

a) for the particular case $\tau_A = \tau_S$

$$S/N = \frac{Q_{col}}{\sqrt{K \cdot T \cdot (F - 1) \cdot C_D}} \cdot \frac{\sqrt{1 + m}}{e}. \quad (25)$$

b) for $\tau_A \neq \tau_S$

$$\begin{aligned} S/N &= \frac{Q_{col}}{\sqrt{K \cdot T \cdot (F - 1) \cdot C_D}} \cdot \\ &\cdot \frac{\sqrt{1 + m}}{1 - m} \cdot \left(e^{\frac{m \cdot \ln m}{1 - m}} - e^{\frac{\ln m}{1 - m}} \right). \end{aligned} \quad (26)$$

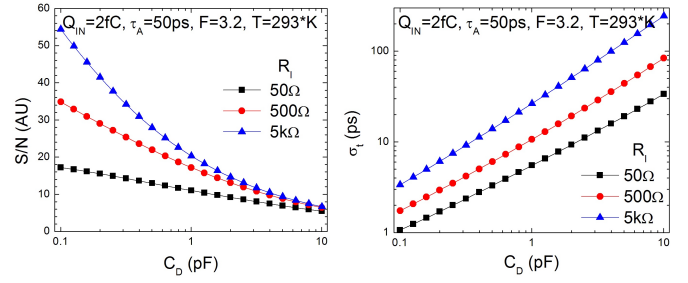


Fig. 4. S/N (left) and σ_t (right) as a function of C_D with R_i as parameter.

In order to obtain σ_t we must calculate the slope SL of $v_{out}(t)$ in the discrimination point, e.g. for simplicity at $t_D = t_M/2$:

$$\begin{aligned} SL(t) &= \frac{d(v_{out}(t))}{dt} \\ &= \frac{Q_{col}}{C_D} \cdot G_0 \cdot \frac{\tau_S}{\tau_S - \tau_A} \cdot \left(\frac{e^{-t/\tau_A}}{\tau_A} - \frac{e^{-t/\tau_S}}{\tau_S} \right). \end{aligned}$$

For $t_D = t_M/2$:

$$\begin{aligned} SL(t_D) &= \frac{Q_{col}}{C_D} \cdot \frac{G_0}{\tau_A} \cdot \frac{1}{1 - m} \\ &\cdot \left(e^{\frac{\ln m}{2 \cdot (1 - m)}} - m \cdot e^{\frac{m \cdot \ln m}{2 \cdot (1 - m)}} \right), \\ \sigma_t &= \frac{\tau_A \cdot \sqrt{K \cdot T \cdot (F - 1) \cdot C_D}}{Q_{col}} \cdot \frac{1 - m}{\sqrt{1 + m}} \\ &\cdot \frac{1}{e^{\frac{\ln m}{2 \cdot (1 - m)}} - m \cdot e^{\frac{m \cdot \ln m}{2 \cdot (1 - m)}}}. \end{aligned} \quad (27)$$

Equations (26) and (27) represent the ideal case of a Dirac excitation where the charge is instantaneously collected. In Fig. 4, S/N (26) and σ_t (27) are plotted as a function of C_D for three values of R_i (50 Ω , 500 Ω , and 5 k Ω). In this evaluation the following parameters have been used: $Q_{col} = 2$ fC, $\tau_A = 50$ ps, $F = 3.2$, $G_0 = 20$.

The S/N increases continuously with decreasing detector capacitance. The influence of the R_i value is minimal for $C_D > 1$ pF ($\tau_S > \tau_A$) and vanishes for $C_D \approx 10$ pF. The ballistic deficit of the preamplifier generates an important loss of the signal amplitude for $C_D < 1$ pF ($\tau_S < \tau_A$), which can be compensated by an increase of R_i , leading to an increase of S/N . The time resolution σ_t degrades linearly with increasing detector capacitance and increasing R_i value.

For the calculations of the dependence of S/N and σ_t on τ_A (Fig. 5), the following parameters have been used: $Q_{col} = 2$ fC, $R_i = 50$ Ω , $F = 3.2$, $G_0 = 20$. Both S/N and σ_t improve significantly for low capacitances and low τ_A values. The bandwidth of the low noise amplifier needed is technologically limited to a few GHz at present (e.g. $BW = 3.018$ GHz, corresponding to a time constant of $\tau_A = 50$ ps). Therefore, the most effective way for improvement is a decrease of the total capacitance.

Fig. 6, 7 and 8 show results of simulations with the APLAC simulation engine [12]. Detectors of capacitances $C_D = 0.1$ pF, 1 pF and 10 pF, respectively, have been assumed, all readout with BBA (Fig. 2 left). The transient signals on the detector (V_S , left scale) are represented by full

symbols, those at the amplifier output (V_A , right scale) by open symbols; a very fast injected charge has been assumed (2 fC in 0.2 ps). The time axis is in logarithmic scale. In each figure three values of R_i are plotted: 50 Ω (squares), 500 Ω (circles) and 5 k Ω (triangles). In all cases, $\tau_A = 50$ ps. The maximum signal amplitude is obtained for minimum detector capacitance $C_D = 0.1$ pF (Fig.6). Nevertheless, it is obvious that all cases show ballistic deficits (note the different Y-scales and remember the amplifier gain $G_0 = 20$).

The minimum ballistic deficit is observed for $C_D = 10$ pF (Fig. 8), but the signals are very small in this case. The design values of C_D and R_i have to be a compromise between the most effective charge collection, the ballistic deficit and the high rate capability of the sensors.

B. Signal Processing at Complete Charge Drift and Collection

According to the Shockley-Ramo theorem, charge movement induces a time dependent current on the detector electrodes. For parallel plate detector geometry and under the assumption of a homogeneously distributed space charge within a scDD, the induced current can be described by the simplified formula (28) [2], [3]:

$$i_{e,h}(t) = \frac{Q_{gen} \cdot v(E)_{e,h}}{d} e^{t/\tau_{eff} - t/\tau_{e,h}}, \quad (28)$$

where Q_{gen} is the generated charge, $v(E)_{e,h}$ is the charge carrier velocity, d is the detector thickness, $\tau_{e,h}$ denotes the lifetime of excess electrons and holes and τ_{eff} is given by

$$\tau_{eff} = \frac{\varepsilon \cdot \varepsilon_0}{q \cdot \mu_{e,h} \cdot N_{eff}}. \quad (29)$$

N_{eff} denotes the net effective fixed space charge in the diamond bulk, ε the diamond permittivity, ε_0 the vacuum permittivity and q the elementary charge. If a negligible amount of space charge is present, the internal electric field is almost constant. If the charge carrier lifetime $\tau_{e,h}$ is longer then the transition time t_{tr} , the carrier drift velocity v_{dr} can be calculated by $v_{dr} = d/t_{tr}$. In this case, a constant induced current is expected for $0 < t < t_{tr}$:

$$i_{e,h}(t) = \frac{Q_{gen}}{t_{tr}} = const.$$

Equations (20) and (21) represent the response of the whole system to the pulse $Q_{col} \cdot \delta(t)$; in order to obtain the response to $1 \cdot \delta(t)$ we must normalize

$$v_{out\delta}(t) = v_{out}(t)/Q_{col}. \quad (30)$$

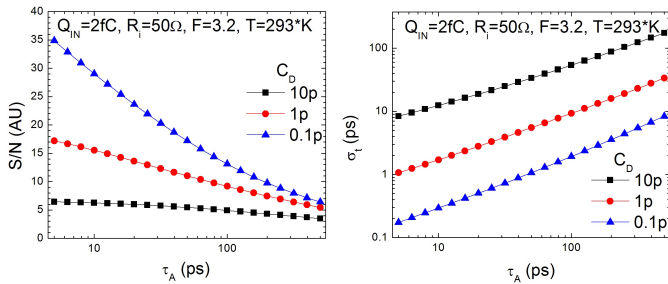


Fig. 5. S/N (left) and σ_t (right) as a function of τ_A with C_D as parameter.

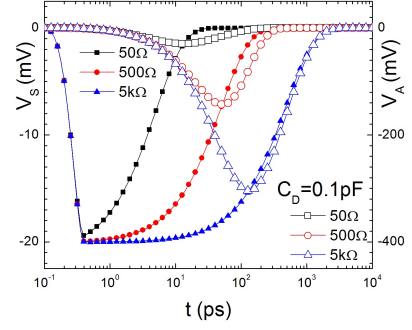


Fig. 6. Simulated signals of a DD with $C_D = 0.1$ pF. Full symbols denote the detector output signals (left ordinate), open symbols the corresponding BBA output signals (right ordinate). Three different values of R_i are considered (50 Ω , 500 Ω , and 5 k Ω) corresponding to $\tau_S = 5$ ps, 50 ps and 500 ps, respectively.

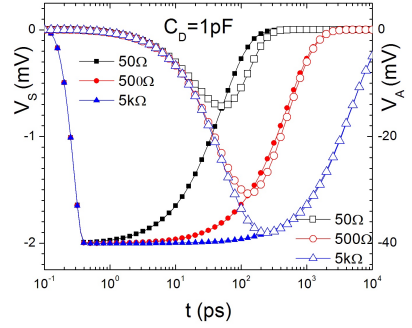


Fig. 7. Same as Fig.6 but for $C_D = 1$ pF and $\tau_S = 500$ ps, 5 ns and 5 ns.

To obtain the amplifier response $v_P(t)$ to $i_{e,h}(t)$, we use the convolution

$$v_P(t) = v_{out\delta}(t) \otimes i_{e,h}(t) = \int_0^t v_{out\delta}(u) \cdot i_{e,h}(t-u) du.$$

For a) $t \leq t_{tr}$

$$v_P(t) = \frac{Q_{gen} \cdot G_0}{C_D} \cdot \frac{\tau_S}{t_{tr}} \cdot \frac{(me^{-t/\tau_A} - e^{-t/\tau_S} + 1 - m)}{1 - m} \quad (31)$$

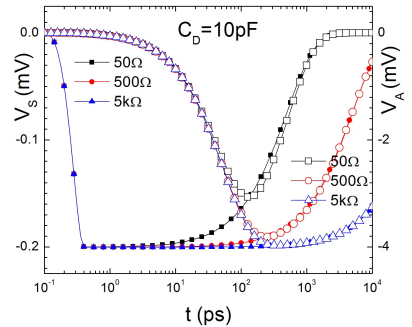


Fig. 8. Same as Fig. 6 but for $C_D = 10$ pF and $\tau_S = 500$ ps, 5 ns and 50 ns.

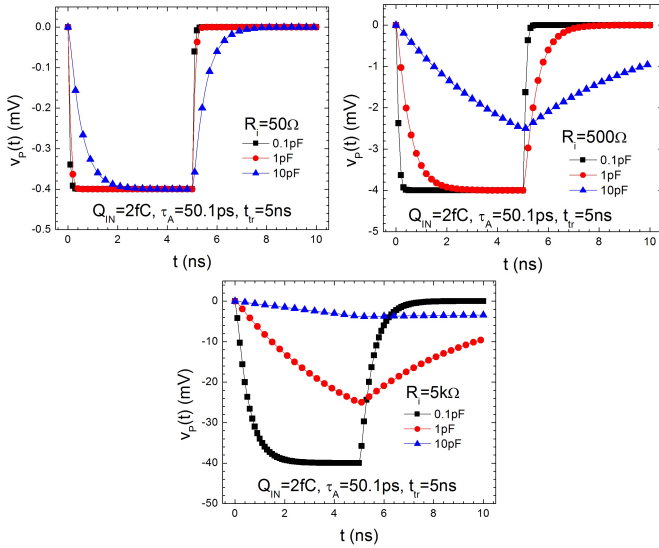


Fig. 9. Transient response of a scDD with $t_{tr} = 5$ ns and three values of C_D (0.1 pF, 1 pF and 10 pF), for $R_i = 50 \Omega$ (upper-left), $R_i = 500 \Omega$ (upper-right) and $R_i = 5 \text{ k}\Omega$ (bottom).

and b) $t > t_{tr}$

$$v_P(t) = \frac{Q_{gen} \cdot G_0}{C_D} \cdot \frac{\tau_S}{t_{tr}} \cdot \left[\frac{-e^{-t/\tau_S} + e^{-(t-t_{tr})/\tau_S}}{1-m} + \frac{m \cdot (e^{-t/\tau_A} - e^{-(t-t_{tr})/\tau_A})}{1-m} \right]. \quad (32)$$

Fig.9 shows the signal response at the output of a BBA (32) for a diamond detector of $C_D = 0.1$ pF (squares), 1 pF (dots) and 10 pF (triangles), respectively. The upper-left figure is calculated for an $R_i = 50 \Omega$, the upper-right for $R_i = 500 \Omega$ and the bottom one for $R_i = 5 \text{ k}\Omega$.

We can estimate the signal amplitude as well as S/N and σ_t for $t = t_{tr}$

$$v_P(t_{tr}) = \frac{Q_{gen} \cdot G_0}{C_D} \cdot \frac{\tau_S}{t_{tr}} \cdot \left[\frac{m \cdot e^{-t_{tr}/\tau_A} - e^{-t_{tr}/\tau_S}}{1-m} + 1 \right]$$

$$S/N = \frac{Q_{gen}}{\sqrt{K \cdot T \cdot (F-1) \cdot C_D}} \cdot \frac{\sqrt{1+m}}{1-m} \cdot \frac{\tau_S}{t_{tr}} \cdot \left(-e^{-t_{tr}/\tau_S} + m \cdot e^{-t_{tr}/\tau_A} + 1 - m \right) \quad (33)$$

$$SL(t) = \frac{d(v_P(t))}{dt} = \frac{Q_{gen} \cdot G_0}{C_D \cdot t_{tr}} \cdot \frac{e^{-t/\tau_S} - e^{-t/\tau_A}}{1-m}.$$

This formula has a maximum for $t = t_M$ (22) when $t_D = t_M/2$,

$$SL(t_D) = \frac{Q_{gen}}{C_D} \cdot \frac{G_0}{t_{tr}} \cdot \frac{1}{1-m} \cdot \left(e^{\frac{m \cdot \ln m}{2 \cdot (1-m)}} - e^{\frac{\ln m}{2 \cdot (1-m)}} \right)$$

$$\sigma_t = \frac{t_{tr} \cdot \sqrt{K \cdot T \cdot (F-1) \cdot C_D}}{Q_{gen}} \cdot \frac{1-m}{\sqrt{1+m}} \cdot \frac{1}{e^{\frac{m \cdot \ln m}{2 \cdot (1-m)}} - e^{\frac{\ln m}{2 \cdot (1-m)}}}. \quad (34)$$

We use (33) and (34) to evaluate the most difficult case, i.e. close to the detection of relativistic protons. The following parameters have been used in Fig. 10: single crystal with

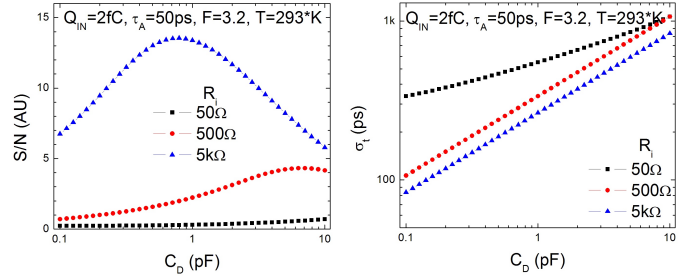


Fig. 10. S/N ratio (left) and σ_t (right) as a function of C_D for three R_i values.

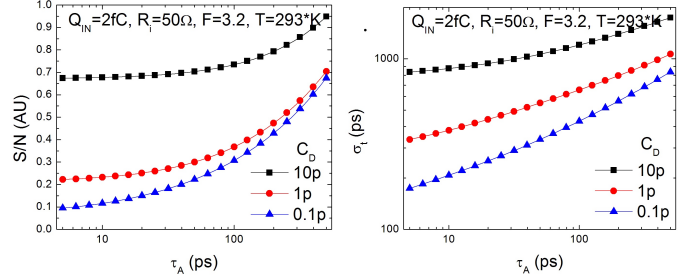


Fig. 11. S/N ratio (left) and σ_t (right) as a function of τ_A , for three values of C_D .

$t_{tr} = 5$ ns, $Q_{col} = 2$ fC, $\tau_A = 50$ ps, $F = 3.2$, $G_0 = 20$, $t_{tr} = 5$ ns. The S/N is less than 1 for any C_D if $R_i = 50 \Omega$ (left). The increase of R_i to 500Ω allows a $S/N > 3$ for $C_D > 2$ pF and shows a maximum for $C_D \approx 9$ pF, when $\tau_S = R_i C_D = 4.5$ ns $\approx t_{tr}$. In the case of $R_i = 5 \text{ k}\Omega$, an optimum situation can be reached for $C_D \approx 0.9$ pF when $\tau_S = 4.5$ ns $\approx t_{tr}$.

Concluding, the S/N has an optimum for $\tau_S \approx t_{tr}$ i.e. when the detector time constant equals the carrier drift time.

σ_t has also a strong dependence on C_D , hence the decrease of the detector capacitance is mandatory. Fig. 11 demonstrates that in the case of $R_i = 50 \Omega$ there is no way to obtain a reasonable S/N and σ_t for fast protons by selecting values for τ_A and C_D .

IV. APPLICATIONS

Over the past years we have designed and constructed a number of SDs for various experiments at GSI. The present material is meant as a comprehensive description of the work we have performed. Some parts may have been presented elsewhere, in particular details of our FEE designs: these cases are properly referenced.

In the following, we give a short overview of these designs and the test results obtained with relativistic beams ranging from protons to tantalum ions. The results of the model simulations presented above served as a guideline for the various projects, especially for the design of proton detectors.

A new diamond SD for the FOPI (FOur PI) detector [13], was planned to replace the standard plastic scintillation start detector. At that time only pcDDs were available in the necessary size; for readout, discrete amplifiers (FEE-1-cards [11]) were used. The results were more than encouraging;

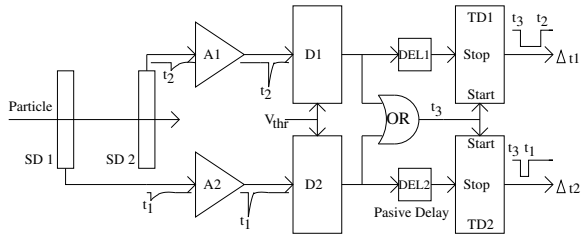


Fig. 12. Circuit for the measurement of the time resolution of SDs. Two identical detector channels are used (see text).

excellent time resolutions have been obtained. Details are described in section IV-A.

Hence, we began to design an even larger system, which included also beam-halo detectors surrounding the central SD (subsection B). The influence of all relevant capacitances to the resolution was demonstrated in the model results; so we tried to reduce the external capacitances by replacing the discrete FEE through the newly developed ASIC PADI-1. It houses three channels designed in a spirit very close to that of the discrete FEE-1 amplifiers [14]. This allowed placing the diamond SD directly on a printed-circuit board, which carries also the amplifier and discrimination system in very close environment.

Considering the model results and the resolutions reached with heavy ions it was obvious that decent results for protons would clearly need single-crystal instead of polycrystalline material. The available areas of about 22 mm² would present already too large capacitance, so the surface had to be segmented and the amplifier had to be placed extremely close to the electrodes. Different technical approaches are described in subsections C and D; this last design was developed to be used in the HADES experiment [15] at GSI.

The time resolutions of the various DD/FEE assemblies have always been measured in the following way: two identical SDs were placed one behind another in the direct beam; in a special experiment the second sensor was replaced by a fast scintillation counter. The generalized setup is shown in Fig. 12. The signals of the two SDs were processed by FEE, which was housing an amplifier (A) followed by a leading edge discriminator (D). The OR signals provide the common start signal of the Time-to-Digital Converters (TD1, TD2) and two passively delayed signals (DEL) stop the individual TD channels. The time-difference spectrum (i.e. the histogram of the time difference $t_D = \Delta t_1 - \Delta t_2 = t_1 - t_2$ can be approximated with a normal distribution of standard deviation σ_{TD} . Assuming equal contributions of the two identical SDs, the time resolution of one channel is given by $\sigma_t = \sigma_{TD}/\sqrt{2}$.

Since the total capacitance of the setup is of high importance, we discuss C_D in the following in more detail. The capacitance of a round disk capacitor of radius a , thickness d , and dielectric constant ϵ_r can be calculated according to [16]:

$$C_D = \frac{a^2 \pi \epsilon_0 \epsilon_r}{d} \left\{ 1 + \frac{2d}{\pi \epsilon_r a} \left[\ln \left(\frac{a}{2d} \right) + (1.41 \epsilon_r + 1.77) + \right. \right.$$

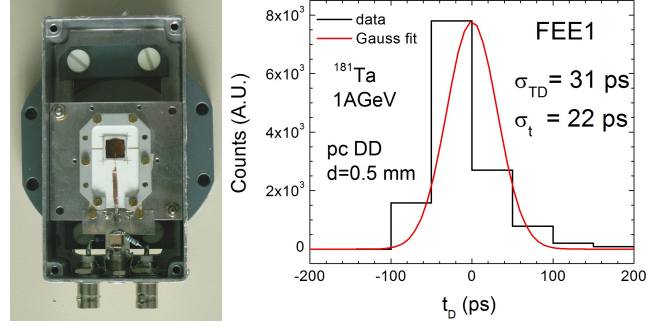


Fig. 13. The pcDD set used in a ¹⁸¹Ta beam of 1 A GeV (left). The time difference spectrum measured between two identical detectors (right). The time resolution is 22 ps.

$$\left. + \frac{d}{a} (0.268 \epsilon_r + 1.65) \right\}. \quad (35)$$

The first term represents the bulk capacitance defined only by the two circular electrodes; the fringe fields are described by the other terms and account for up to 20% of C_D . For other shapes and geometries, the share of the fringe capacitance may be even higher; it can be estimated on the basis of approximating formulae or by simulation programs. We decided to *measure* the total detector capacitance C_D ; we used Boonton Capacitance Meter Model 72BD. In the following, we will specify C_D by two values: the estimated value C_{DE} , which ignores the fringe effects and the measured value C_{DM} , which is the total value including all assembly capacitances: the detector bulk capacitance plus fringe as well as the parasitic and the preamplifier input capacitances (not biased) for the FEE located close to the DD.

A. Start Detectors for Heavy Ions

As a new in-beam SD for the FOPI experiment, a pcDD has been mounted in the center of an aluminum box (Fig.13, left photo); metallized mylar entrance and exit windows close the box. The crystal has an area of 10 mm x 10 mm, a thickness of 0.5 mm, and it is fixed on a ceramic substrate. Each surface is covered by a round Cr/Au-electrode of 8 mm diameter ($C_{DE} = 5.14$ pF, $C_{DM} = 6.8$ pF), one being used as HV-electrode, the other for readout (cf. the two BNC connectors at the bottom of the box). For timing tests, two FEE-1 cards [11], each consisting of four discrete channels of high-frequency amplifiers followed by fast leading edge discriminators, are used to readout two identical detector modules placed one behind the other perpendicular to the beam direction.

Using ¹⁸¹Ta beam of 1 A GeV, a time resolution $\sigma_t \approx 22$ ps was measured (Fig. 13, right plot); a similar value ($\sigma_t \approx 28$ ps) has been obtained with ²⁷Al ions of 2 A GeV.

B. An Integrated Universal Beam Monitor and Start Detector for Heavy-Ion Experiments

After the positive results obtained from our first SD test (subsection IV-A) we designed a new assembly, in order to meet all the requirements of a start system of the FOPI experiment. The size of the pcDD was as large as 20 mm

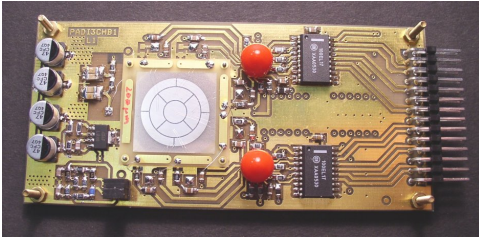


Fig. 14. Board comprising the 20 mm x 20 mm pcDD and the complete electronics including two ASIC chips. The DD is divided into nine separate segments for timing measurement and beam monitoring (see text for details).

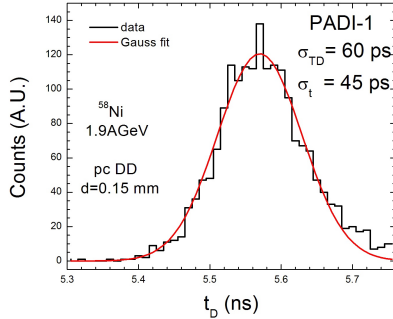


Fig. 15. Time difference spectrum measured with the central pad of the DD of Fig. 14 in coincidence with a plastic scintillation detector. The DD plus FEE contributes with $\sigma_t = 45$ ps to the total $\sigma_{TD} = 60$ ps of the ToF spectrum.

x 20 mm; it is only 0.15 mm thick in order to reduce beam straggling and reactions in the detector material. It has identical aluminum contacts on front and back side, consisting of a central electrode of 5.5 mm diameter ($C_{DE} = 7.7$ pF, $C_{DM} = 9.2$ pF) for the start signal, four surrounding sectors for beam-profile measurements or beam-halo control, plus another segmented outermost ring (cf. Fig. 14). The latter serves merely as a potential ring to guarantee the field homogeneity along the borders of the beam-halo electrodes.

In order to minimize the capacitances the FEE is equipped with two PADI-1 chips [14]; all components are mounted together with the DD on a common printed circuit board in a dense configuration.

Each PADI-1 chip has three preamplifier-discriminator channels followed by digital buffers, which are used for readout and processing of the signals of the five detector segments; the digitization is performed with external units.

This setup has been used in an experiment with a 1.9 A GeV ^{58}Ni beam. The time resolution was measured in reference to the standard FOPI start detector, i.e. a plastic scintillation detector, read out by two fast phototubes [13]; the resolution of each sensor can be determined independently. From the measured total $s_{TD} = 60$ ps (Fig. 15), $\sigma_t = 45$ ps are attributed to the diamond setup.

The rate capability of PADI-1 has been investigated in a beam test experiment with carbon ions using a scDD of 3 mm x 3 mm area. The diamond sensor of 0.3 mm thickness was metallized with four circular pad electrodes on both sides, each of 1.2 mm diameter and of capacitances $C_{DE} = 0.18$ pF

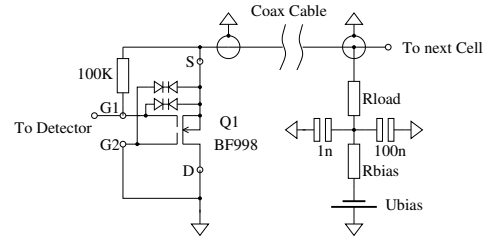


Fig. 16. Schematics of the MOS buffer.

and $C_{DM} = 2.9$ pF, respectively. We observed a linear dependence of the detected rate on the beam intensity up to 1.35×10^8 ions/spill. For details see [17], [18].

C. Start Detectors for Relativistic Light Ions and Protons Featuring a Simple MOS Buffer.

The model calculations as well as the experimental results described so far showed clearly that good time resolutions for light ions, and in particular protons, demand additional design improvement: one has to consequently minimize all relevant capacitances of the assemblies, to increase the preamplifier input impedance, and, above all, to use single-crystal diamond as detector material.

For a first beam test, the electrodes of two scDDs (of area = 4 mm x 4 mm and thickness $d = 0.4$ mm) have been segmented into four sectors, each of those directly bonded to the corresponding input of its amplifier, which was located in close proximity of the sensor. We have chosen the BFR998 double-gate MOS transistor which is often used in VHF/UHF amplifiers since it has a very good noise figure (typically 0.6 dB@200 MHz and 1 dB@800 MHz) and a BW = 1 GHz. In addition, it has an input capacitance $C_i = 1.2$ -2.4 pF, an output capacitance $C_{out} = 1$ pF, a feedback capacitance $C_{G1D} < 25$ fF and a transconductance of $g_m \approx 25$ mA/V. The DC bias and the detector signal are transmitted through a 50 Ω coaxial cable to a modified version of the FEE-1 [11] which contains also the biasing circuit. The simple MOS buffer (MB) circuit (Fig. 16) allows to easily adjusting the detector time constant (in this case $\tau_S \approx (C_{DE} + 2 \text{ pF}) \times 100 \text{ k}\Omega$). The resulting capacitances per sector were $C_{DE} = 0.2$ pF and $C_{DM} = 3.3$ pF.

Fig. 17 shows the time difference spectrum measured with two well-aligned opposite sectors of the two quadrant sensors, which were mounted in short distance between each other perpendicular to a ^6Li beam of 1.8 A GeV. The time resolution obtained was $\sigma_t = 55$ ps.

However, this simple MOS buffer solution has two drawbacks: $C_i (\approx 2 \text{ pF})$ is not sufficiently low, and, since the gain is below 1.0, the noise of the next cell must be low too.

D. The new scDD Proton Start Detector for HADES

In the design described in the following, the above disadvantages have been eliminated. For the new proton start detector for the HADES spectrometer at GSI, the segmentation of the sensor electrode has been driven even further: the scDD of 4.7 mm x 4.7 mm area and $d = 0.5$ mm thickness is segmented

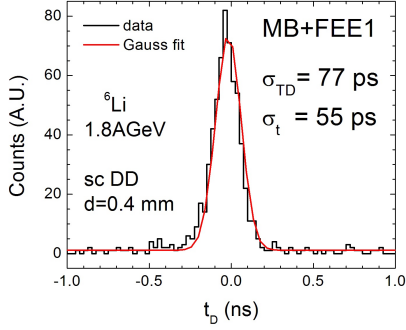


Fig. 17. Time difference spectrum measured with relativistic ${}^6\text{Li}$ ions of 1.8 A GeV using the MOS buffer plus the FEE-1 card and scDD sc3 (Table II).

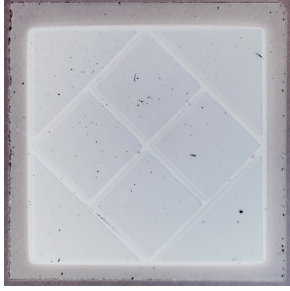


Fig. 18. The new SD of HADES is a scDD of 4.7 mm x 4.7 mm size and a thickness of 500 μm ; it is segmented in eight pads.

in eight pads (Fig. 18) yielding $C_{DE} = 0.142$ pF and $C_{DM} = 1.5$ pF. The new FEE consists of a low capacitance broadband amplifier (LCB) for the first stage mounted close to the sensor [19].

Fig. 19 shows the used FEE schematic. The low capacitance broadband amplifier (LCB) consists of a 14 GHz wideband silicon planar transistor mounted in common-emitter configuration. It is mounted as close as possible to the corresponding pad of the segmented electrode. This transistor has a low noise figure ($NF = 1$ dB) as well as low collector-base ($C_{CBS} = 0.13$ pF) and emitter-base capacitances ($C_{EBS} = 0.22$ pF). The biasing resistor is divided in three elements to minimize the total parasitic capacitance. The collector load resistor is located at the input of the next cell.

The left-hand side photograph of Fig. 20 shows the FEE board with its eight LCB channels before the mounting and bonding of the DD shown in Fig. 19 into the central hole. The identical electronics scheme was used to test a second SD assembly, which was consisting of a sensor with one

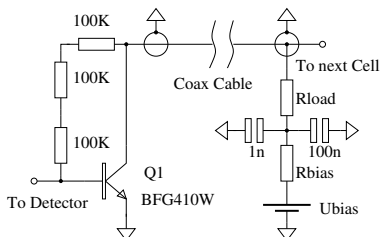


Fig. 19. Schematics of the low capacitance broadband amplifier FEE.

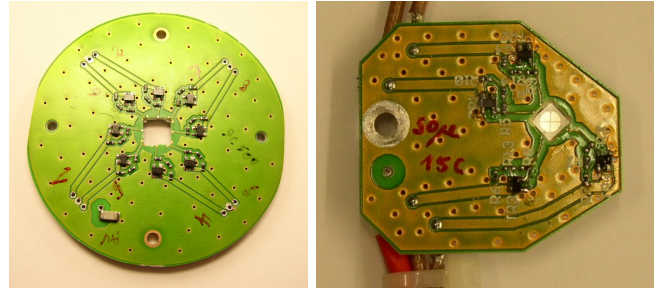


Fig. 20. Mounting details of the LCB: at left is shown the PCB with 8 channels used in the proton beam test and on the right one, a quadrant-SD (sc4, Table II) surrounded by four LCB amplifiers, as used in a ${}^6\text{Li}$ beam test.

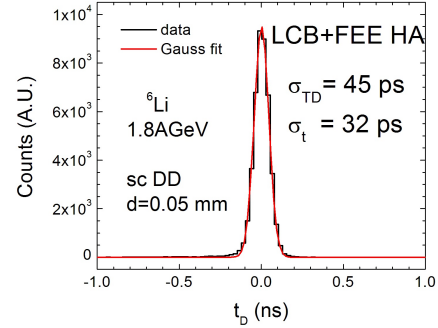


Fig. 21. Time resolution measured with ${}^6\text{Li}$ ions of 1.8 A GeV between two segments of two different scDD (sc4, Table II), read out with the low capacitance broadband amplifiers (LCB) developed for the HADES spectrometer.

electrode segmented in four sectors (quadrant detector sc4, Table II). Its board is shown on the right side of Fig. 20 with the SD mounted in the right hole. The collectors of the LCB amplifiers are connected through micro strip lines to coaxial cables, which transmit the signals to the next amplifier cells. The PCB material is Rogers 4003C, a high-frequency material (glass-reinforced hydrocarbon and ceramics) with a dielectric constant $\epsilon_r = 3.38 \pm 0.05$. In order to minimize the detector fringe capacitance, the ground plane has a circular groove cut around the detector.

Two identical single-crystal diamond quadrant sensors (cs4, Table II) were tested with ${}^6\text{Li}$ ions of 1.8 A GeV and a time resolution $\sigma_t = 32$ ps (Fig. 21) was achieved. This can be compared to the 55 ps measured in the same beam test with the simplified MOS-buffer FEE type of subsection IV-C (Fig. 17). The eight-sector SD delivered with protons of 3.5 GeV a resolution $\sigma_t = 117$ ps, which is the best proton value, reached so far [19].

V. SUMMARY AND CONCLUSIONS.

In this paper we describe a variety of detector systems consisting of diamond detectors and their front-end electronics, which we have designed and built as in-beam start detectors for existing and future GSI experiments. They should be able to cope with all beams of relativistic ions including protons, the detection of which is a particular challenge because of the very low primary charge generated in the detector material.

TABLE I
TIME RESOLUTIONS OF VARIOUS ASSEMBLIES TESTED WITH VARIOUS
BEAMS AND BEAM ENERGIES

Ion: Type, Energy	FEE type	σ_t (ps)	EFF (%)	DD No.
p, 1.25 GeV	TCSA+FEE-1	330	96	sc1
p, 3.5 GeV	LCB+FEE HA	117	94	sc2
${}^6\text{Li}$, 1.8 A GeV	MB+FEE-1	55	no	sc3
${}^6\text{Li}$, 1.8 A GeV	LCB+FEE HA	32	no	sc4
${}^{27}\text{Al}$, 2 A GeV	FEE-1	28	92	pc1
${}^{58}\text{Ni}$, 1.9 A GeV	PADI-1	45	no	pc2
${}^{181}\text{Ta}$, 1 A GeV	FEE-1	22	94	pc3

TABLE II
DETAILS OF THE TESTED DD

DD No.	Size (mm ²)	d (mm)	No. of Pads	Pad Area (mm ²)	C_{DE} (pF)	C_{DM} (pF)
sc1	4 x 4	0.5	4	1.69	0.165	1.2
sc2	4.7 x 4.7	0.5	8	1.46	0.142	1.5
sc3	4 x 4	0.4	4	1.69	0.2	3.3
sc4	3.5 x 3.5	0.05	4	1.43	1.4	2.5
pc1	10 x 10	0.5	1	52.8	5.14	6.8
pc2	20 x 20	0.15	9	23.8	7.7	9.2
pc3	10 x 10	0.5	1	52.8	5.14	6.8

In parallel, we have performed extensive model calculations to estimate the dependence of the signal-to-noise ratio S/N and the time resolution σ_t on various parameters. The computation results presented in detail in section III, together with the measured resolutions of scDDs and pcDDs, show that a minor decrease of the total system capacitance C_D and an increase of the amplifier input resistance R_i alone are not sufficient for proton detection. C_D has to be minimized by a) an extremely careful design of the DD-FEE assembly, where especially the first stage of the FEE has to be positioned as close as possible to the DD, b) a minimization of fringing detector capacitances (for which the mounting PCB should have the ground layers at a few mm distance) and c) by segmentation of the DD into single pads, not exceeding a few mm². When C_D is minimized, the input resistance R_i can be adjusted to obtain the optimum condition for S/N : $\tau_S \approx t_{tr}$. In addition, one should use only single-crystal detectors, which collect almost 100% of the primary charge.

Table I summarizes the experimental results obtained with the diamond detectors described in Table II: the time resolutions σ_t achieved with the presented DD-FEE assemblies in various beam tests with relativistic ions of different energies, and the detection efficiencies (EFF, if measured).

The tested scDDs and pcDDs are labeled sci and pci with i as running number; the FEE types are given as they are denominated in the text. Along with the DD-FEE assemblies described in section IV, we present the results of an early test performed with a scDD assembly (sc1, Table II) equipped with a FEE consisting of a fast charge sensitive amplifier (TCSA) [20] as a first stage followed by a FEE-1 card.

The pc diamond SDs read out with FEE-1 or PADI-1 ASICs deliver satisfying resolutions for relativistic heavy-ions in the order of $\sigma_t \approx 45$ ps. The sc diamond SDs have demonstrated time resolutions $\sigma_t < 60$ ps with ${}^6\text{Li}$, ${}^{12}\text{C}$ and ${}^{27}\text{Al}$ ions.

The best value obtained for relativistic protons was

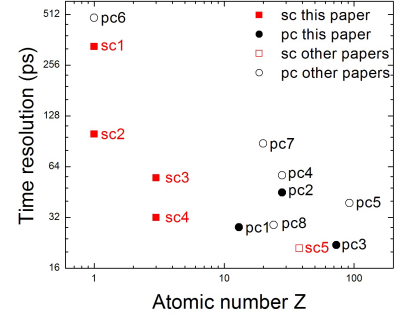


Fig. 22. Comparison of measured time resolutions presented in this paper (full symbols) and other literature values (open symbols) for fast charged particles from protons to U; square symbols denote scDD, round symbols denote pcDD. The added external values for pc-4, pc-5, pc-6, pc-7, pc-8 and sc-5 are taken from the references [21], [21], [22], [23], [24], and [25], respectively.

$\sigma_t \approx 117$ ps. This was achieved by segmentation of the electrodes and reduction of parasitic capacitances and amplifier input capacitance. In addition, the amplifier input impedance, and due to this the detector time constant, had to be increased. The present resolution is not satisfying yet in the light of the design goal defined in the introduction. Further improvements are conceivable; however, both on the side of electronics and on the material side (e.g. the novel CVD diamond material, grown on large iridium wafers has a good perspective for future timing applications [5]).

In order to put our results in a larger context, we present the obtained values in Fig. 22 together with all other DD results found in the literature. Ions from proton to ${}^{238}\text{U}$ and both sc- and pc-material were used. It is obvious that our results have widened the field considerably; to our knowledge they are presently the state of the art in timing with diamond detectors.

ACKNOWLEDGMENT

This work is partially supported by the European FP6 Project RII3-CT-2004-506078 and by the German BMBF under the project number 06HD190i. We express our gratitude to G. May and M. Träger for indefatigable cooperation and technical support. Special thanks from all of us go to P. Moritz for the excellent design of the DBA amplifiers, and in particular to C. Kozhuharov, C. J. Schmidt and H. Bozdog for many fruitful discussions regarding this manuscript.

REFERENCES

- [1] E. Berdermann and M. Ciobanu, "CVD-Diamond Detectors for Experiments with Hadrons, Nuclei and Atoms" in *CVD Diamond for Electronic Devices and Sensors*, R. S. Sussmann, Ed. New York: Wiley, 2009, pp. 227-255.
- [2] H. Pernegger, S. Roe, P. Weilhammer, V. Eremin, H. Frais-Kolbl, and E. Griesmayer *et al.*, "Charge-carrier properties in synthetic single-crystal diamond measured with the transient-current technique", *J. Appl. Phys.*, vol. 97, p. 073704, 2005.
- [3] M. Pomorski, "Electronic properties of single crystal CVD diamond and its suitability for particle detection in hadron physics experiments" Wolfgang von Goethe University, Frankfurt am Main, Germany, 2008. Available online: http://www-norhdia.gsi.de/publications/pomorski_thesis_final_LQ.pdf.

- [4] W. Adam, W. de Boer, E. Borch, M. Bruzzi, C. Colledani, and P. D' Angelo *et al.*, "Radiation hard diamond sensors for future tracking applications", *Nucl. Instr. Meth. A*, vol. 565, pp. 278-283, 2006.
- [5] E. Berdermann, M. Pomorski, W. de Boer, M. Ciobanu, S. Dunst, and C. Grah *et al.*, "Diamond detectors for hadron physics research", *Diamond Related Mater.*, vol. 19, pp. 358-367, 2010.
- [6] P. Moritz, E. Berdermann, K. Blasche, H. Stelzer, and B. Voss, "Broad-band electronics for diamond detectors", *Diamond Related Mater.*, vol. 10, pp. 1770-1777, 2001.
- [7] H. Spieler, SLUO Lecture Series 1998. Available online: http://www-group.slac.stanford.edu/sluc/lectures/detector_lecture_files/detectorlectures_10.pdf.
- [8] H. Spieler, *Radiation Detectors and Signal Processing*, Lecture series pres. at Univ. of Heidelberg, Germany 2005. Available online: http://www-physics.lbl.gov/~spieler/Heidelberg_Notes_2005/pdf/IV_Signal_Processing.pdf.
- [9] H. Spieler, "Fast timing methods for semiconductor detectors", *IEEE Trans. Nucl. Sci.*, vol. 29, no. 3, pp. 1142-1158, Jun. 1988.
- [10] A. Pullia and E. Gatti, "Optimal filters with constant-slope crossover and finite width for pulse-timing measurements", *IEEE Trans. Nucl. Sci.*, vol. 49, no. 3, pp. 1170-1176, Jun. 2002.
- [11] M. Ciobanu, A. Schüttauf, E. Cordier, N. Herrmann, K. D. Hildenbrand, and Y. J. Kim *et al.*, "A front-end electronics card comprising a high gain/high bandwidth amplifier and a fast discriminator for time-of-flight measurements", *IEEE Trans. Nucl. Sci.*, vol. 54, no. 4, pt. 3, pp. 1201-1206, Aug. 2007.
- [12] The APLAC simulator, Available online: <http://web.awrcorp.com/Usa/Products/APLAC>.
- [13] A. Gobbi, J. P. Alard, G. Augustinski, Z. Basrak, N. Bastid, and I. M. Betayev *et al.*, "A highly-segmented ΔE -time-of-flight wall as forward detector of the 4π -system for charged particles at the SIS/ESR accelerator", *Nucl. Instr. Meth. A*, vol. 324, pp. 156-176, 1993.
- [14] M. Ciobanu, N. Herrmann, K. D. Hildenbrand, M. Kiš, and A. Schüttauf, "PADI, a fast Preamplifier – Discriminator for time-of-flight measurements", in *Proc. IEEE Nucl. Sci. Symp.*, Dresden, Germany, 2008, vol. N30-18, pp. 2018-2024.
- [15] G. Agakishiev, C. Agodi, H. Alvarez-Pol, E. Atkin, E. Badura, and A. Balanda *et al.*, "The high-acceptance dielectron spectrometer HADES", *Eur. Phys. J. A* vol. 41, pp. 243-277, 2009.
- [16] W. C. Chew and J. A. Kong, "Effects of fringing fields on the capacitance of circular microstrip disk", *IEEE Trans. on Microw. Theory Techn.*, vol. MTT-28, no. 2, pp. 98-104, Feb. 1980.
- [17] M. Rebisz, "Alternative methods for heavy-ion therapy dosimetry" Ph.D. dissertation, Ruprecht-Karls Universität Heidelberg, Germany, 2007. Available online: <https://www.gsi.de/documents/DOC-2008-Apr-5-1.pdf>.
- [18] M. Rebisz-Pomorska, M. Ciobanu, M. Kiš, M. Pomorski, and B. Voss, "Diamond detectors for the monitoring of carbon-ion therapy beams", *Nucl. Instr. Meth. A*, vol. 620, pp. 534-539, 2010.
- [19] J. Pietraszko, L. Fabbietti, W. Koenig, and M. Weber, "Diamond as timing detectors for minimum-ionizing particles: The HADES proton-beam monitor and START signal detectors for time of flight measurements", *Nucl. Instr. Meth. A* vol. 618, pp. 121-123, 2010.
- [20] M. Ciobanu, N. Herrmann, K. D. Hildenbrand, T. I. Kang, M. Kiš, and A. Schüttauf, "A charge sensitive amplifier for time and energy measurements", in *Proc. IEEE Nucl. Sci. Symp.*, Dresden, Germany, 2008, vol. N30-20, pp. 2028-2032.
- [21] E. Berdermann, K. Blaske, P. Moritz, H. Stelzer, B. Voss, and F. Zeytouni, "First applications of a CVD-diamond detectors in heavy-ion experiments", *Nucl. Phys. B (Proc. Suppl.)*, vol. 78, pp. 533-539, 1999.
- [22] M. Mikuž, V. Cindro, I. Dolenc, H. Kagan, G. Kramberger, and H. Frais-Kölbl *et al.*, "The ATLAS beam conditions monitor", in *Proc. IEEE Nucl. Sci. Symp.*, Honolulu, Hawaii, 2007, vol. N31-7, pp. 1914-1917.
- [23] A. Lohstroh, F. Schirru, B. S. Nara Singh, L. Scruton, M. Bentley, S. P. Fox *et al.*, "Polycrystalline diamond detectors for time of flight measurements of high energy ion beams", presented at *IEEE Nucl. Sci. Symposium*, Knoxville, Tennessee, 2010, private communication.
- [24] A. Stolz, M. Behrven, M. Regmi, and B. Golding, "Heteroepitaxial diamond detectors for heavy ion beam tracking", *Diamond Related Mater.*, vol. 15., pp. 807-810, 2006.
- [25] E. Berdermann, K. Blasche, P. Moritz, H. Stelzer, and B. Voss, "The use of CVD-diamond for heavy-ion detection", *Diamond Related Mater.*, vol. 10, pp. 1770-1777, 2001.